Trans Indian Inst Met (2015) 68(3):433–442
DOI 10.1007/s12666-014-0472-x

TECHNICAL PAPER

TP 2868

Growth Kinetics of the Fe_2B Coating on AISI H13 Steel

M. Keddam · M. Ortiz-Domínguez · M. Elias-Espinosa · O. Damián-Mejía · A. Arenas-Flores · O. A. Gómez-Vargas · M. Abreu-Quijano · Jorge Iván Aldana-González · J. Zuno-Silva

Received: 28 June 2014 / Accepted: 28 October 2014 / Published online: 5 December 2014

Abstract A kinetic model was suggested to study the growth kinetics of Fe_2B layers on AISI H13 steel via the pack-boriding method in the temperature range of 1,123–1,273 K. This model was based of the principle of mass conservation at the (Fe_2B/substrate) interface where the boride incubation time was independent of the boriding temperature. The model was also validated experimentally by comparing the experimental Fe_2B layers thicknesses with the predicted values at 1,173 K during 7 h, 1,223 K during 5 h, 1,253 K during 2 h and 1,273 K for 3 h. The Fe_2B layers grown on AISI H13 steel were characterized by use of the following experimental techniques: optical microscopy, scanning electron microscopy, energy dispersive X-ray spectroscopy and X-ray diffraction analysis. In addition, a contour diagram describing the evolution of Fe_2B layers as a function of the boriding parameters (time and temperature) was proposed. Finally, the boron activation energy for AISI H13 steel was estimated as 233 kJ mol^{-1} on the basis of our experimental results. This value of energy was compared with the literature data.

Keywords Boriding · Iron boride · Incubation time · Kinetic model · Activation energy

List of Symbols

v	Boride layer thickness (m)
t_v	Effective growth time of the Fe_2B layer (s)
t	Treatment time (s)
$t_0^{Fe_2B}$	Boride incubation time (s)
Q_{Fe_2B}	Activation energy of the system (J mol^{-1})
$C_{up}^{Fe_2B}$	Upper limit of boron content in Fe_2B (=60 × 10^3 mol m^{-3})

M. Keddam (✉)
Laboratoire de Technologie des Matériaux, Faculté de Génie Mécanique et Génie des Procédés, USTHB, B.P. No. 32, El-Alia, Bab-Ezzouar, 16111 Algiers, Algeria
e-mail: keddam@yahoo.fr

M. Ortiz-Domínguez · M. Abreu-Quijano · J. Zuno-Silva
Escuela Superior Cd. Sahagún, Universidad Autónoma del Estado de Hidalgo, UAEH, Carretera Cd. Sahagún-Otumba s/n, 43990 Pachuca, Hidalgo, Mexico

M. Elias-Espinosa
Instituto Tecnológico y de Estudios Superiores de Monterrey-ITESM Campus Santa Fe, Av. Carlos Lazo No. 100, Del. Álvaro Obregón, CP 01389 Mexico, D.F., Mexico

O. Damián-Mejía
Instituto de Investigación en Materiales, Universidad Nacional Autónoma de México-UNAM, Circuito Exterior, s/n Ciudad Universitaria, CP 04510 Coyoacán, D.F., Mexico

A. Arenas-Flores
Centro de Investigación en Materiales y Metalurgia, Universidad Autónoma del Estado de Hidalgo, Ciudad Universitaria Pachuca-Tulancingo km. 4.5, Pachuca, Hidalgo, Mexico

O. A. Gómez-Vargas
Instituto Tecnológico de Tlalnepantla-ITTLA, Av. Instituto Tecnológico, S/N. Col. La Comunidad, CP 54070 Tlalnepantla de Baz, Estado de México, Mexico

J. I. Aldana-González
Universidad Tecnológica de México, Blvd. Calacoaya No. 7, Col. La Ermita, 52970 Atizapán de Zaragoza, Estado de México, Mexico

$C_{low}^{Fe_2B}$	Lower limit of boron content in Fe_2B (=59.8 × 10^3 mol m^{-3})
C_{ads}^{B}	Adsorbed boron concentration in the boride layer (mol m^{-3})
$a_1 = C_{up}^{Fe_2B} - C_{low}^{Fe_2B}$	Homogeneity range of the Fe_2B layer (mol m^{-3})
$a_2 = C_{low}^{Fe_2B} - C_0$	Miscibility gap (mol m^{-3})
C_0	Terminal solubility of the interstitial solute ($\approx$0 mol m^{-3})
$C_{Fe_2B}[x(t)]$	Boron concentration profile in the Fe_2B layer (mol m^{-3})
$erf(x/2\sqrt{D_{Fe_2B}t})$	Error function (it has no physical dimensions)
v_0	Initial Fe_2B layer (m)
ε	Normalized growth parameter for the (Fe_2B/substrate) interface (it has no physical dimension)
D_{Fe_2B}	Diffusion coefficient of boron in the Fe_2B phase (m^2 s^{-1})
$J_i[x(t)]$, (with i = Fe_2B and Fe)	Fluxes of boron atoms in the (Fe_2B/substrate) interface boundary (mol m^{-2} s^{-1})

1 Introduction

Boriding is a thermochemical treatment widely used to harden the surface of steel and alloys. It is defined as an enrichment of the surface of a workpiece with boron by thermodiffusion [1]. In the case of steels or Armco iron, this process forms very hard and wear resistant iron borides (i.e. Fe_2B and FeB) on the surface. It modifies the properties of ferrous alloys by improving the surface hardness, wear resistance and corrosion resistance [2]. The possibility of formation of Fe_2B and/or FeB boride layers depends on the boron activity in the reactive medium and the chemical composition of the substrate as well as on the boriding parameters (time and temperature).

Boriding of ferrous alloys is generally realized in the temperature range of 800–1,050 °C for treatment times ranging from 0.5 to 10 h, by use of a boron source in different states such as solid powder, paste, liquid, gas and plasma. The widespread used method is pack-boriding (similar to pack-carburizing) because of its technical advantages [3]. Generally, the commercial boriding mixture is composed of boron carbide (B_4C) as donor, KBF_4 as an activator and silicon carbide (SiC) as a diluent to control the boriding potential of the medium. The morphology of the boride layer is influenced by the presence of alloying elements in the matrix. Saw-tooth shaped layers are obtained in low-alloy steels or Armco iron whereas in high-alloy steels, the interfaces tend to be flat. A monophase Fe_2B layer is desirable for the intended applications in industry because of difference between the specific volume and coefficient of thermal expansion of boride and the substrate [4, 5]. The modeling of the boriding kinetics is considered as a suitable tool to select the optimum process parameters for obtaining adequate boride layers thicknesses in relation with their practical applications [6]. So, the modeling of the growth kinetics of boride layers has gained much attention to simulate the boriding kinetics during these last decades. Several diffusion models [7–20] were reported in the literature concerning the solid boriding method (paste or powder) with and without the effect of boride incubation times.

In the present study, a kinetic model was suggested to estimate the boron diffusion coefficients through the Fe_2B layers grown on AISI H13 steel. The model was also validated by comparing the Fe_2B layers thicknesses with the predicted values for the borided samples at 1,173 K during 7 h, 1,223 K during 5 h, 1,253 K during 2 h and 1,273 K during 3 h. The obtained boride layers on AISI H13 steel were characterized by means of the following techniques: optical microscopy, scanning electron microscopy coupled to EDS and XRD analysis. The boron activation energy for AISI H13 steel was also estimated in the temperature range of 1,123–1,273 K by use of a kinetic model.

2 The Kinetic Model

The model considers the growth of Fe_2B layer on a saturated substrate with boron atoms as displayed in Fig. 1. The boron potential allows only the formation of a single phase (Fe_2B) on the surface of treated substrate. The $f(x, t)$ function illustrates the boron distribution in the austenite matrix before the nucleation of Fe_2B phase. $t_0^{Fe_2B}$ denotes the incubation time required to form the Fe_2B phase when the saturation state is reached within the substrate with boron atoms. $C_{up}^{Fe_2B}$ is the upper limit of boron content in Fe_2B (=60 × 10^3 mol m^{-3}) while $C_{low}^{Fe_2B}$ represents the lower limit of boron content in Fe_2B (=59.8 × 10^3 mol m^{-3}). $x(t = t) = v$ is the position of the (Fe_2B/substrate) interface as a function of the treatment time or the Fe_2B layer thickness [6, 21, 22].

The boron concentration $(C_{Fe_2B}[x(t), t] = A + B\,erf(x/\sqrt{4D_{Fe_2B}t}))$ in the Fe_2B layer (see Fig. 1) is the solution of Fick's Second Law in a semi-infinite medium, and it depends on the position $x(t)$ and t time (cf. the small homogeneity ranges of about 1 at.% for the Fe_2B layer [23]). A and B are constants to be determined from the initials and boundary conditions of the diffusion problem. It is also assumed that the boron surface concentration and interface concentration do not change during boriding process. The term C_{ads}^{B} is the effective adsorbed boron concentration during the boriding process [24]. From Fig. 1, $a_1 = C_{up}^{Fe_2B} - C_{low}^{Fe_2B}$ defines the homogeneity range of the Fe_2B layer, $a_2 = C_{low}^{Fe_2B} - C_0$ is the miscibility gap [19, 20] and C_0 the boron solubility in the

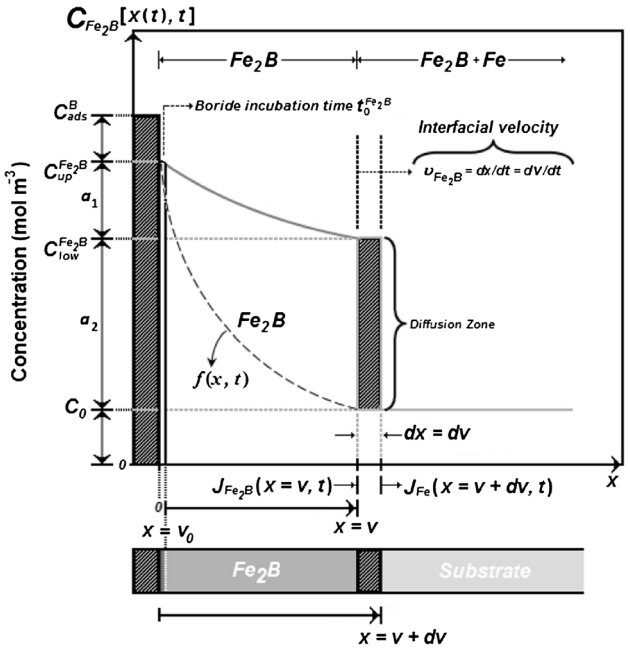

Fig. 1 Schematic boron- concentration profile through the Fe_2B layer

matrix. The diffusion zone underneath the Fe_2B layer can be neglected ($C_0 \approx 0$ mol m^{-3}) [25, 26] due to the lower solubility of boron. The following assumptions are taken into consideration during the formulation of the diffusion model:

- The growth kinetics is controlled by the boron diffusion in the Fe_2B layer.
- The Fe_2B iron boride nucleates after a certain incubation time.
- The boride layer grows because of the boron diffusion perpendicular to the specimen surface.
- Boron concentrations remain constant in the boride layer during the treatment.
- The boride layer is thin compared to the sample thickness.
- A uniform temperature is assumed throughout the sample.
- Planar morphology is assumed for the phase interface.

The initial and boundary conditions for the diffusion problem are represented as:

$$t = 0, \quad x > 0, \text{ with: } C_{Fe_2B}[x(t),\ t = 0] = C_0 \approx 0. \tag{1}$$

Boundary conditions:

$$C_{Fe_2B}\left[x\left(t = t_0^{Fe_2B}\right) = v_0,\ t = t_0^{Fe_2B}\right] = C_{up}^{Fe_2B}$$

(the upper boron concentration is kept constant),

$$\text{for } C_{ads}^B > 60 \times 10^3 \text{ mol m}^{-3}, \tag{2}$$

$$C_{Fe_2B}[x(t = t) = v, t = t] = C_{low}^{Fe_2B}$$

(the boron concentration at the interface is kept constant),

$$C_{ads}^B < 59.8 \times 10^3 \text{mol m}^{-3}, \tag{3}$$

v_0 is a thin layer with a thickness of ≈5 nm that formed during the nucleation stage [27]. Thus v_0 (≈0) when compared to the thickness of Fe_2B layer (v). The mass balance equation at the (Fe_2B/substrate) interface can be expressed by Eq. (4) as follows:

$$\left(\frac{C_{up}^{Fe_2B} + C_{low}^{Fe_2B} - 2C_0}{2}\right)(A \cdot dv) = J_{Fe_2B}(x = v, t = t)(A \cdot dt) - J_{Fe}(x = v + dv, t = t)(A \cdot dt), \tag{4}$$

where A(=1.1) is defined as the unit area and C_0 represents the boron concentration in the matrix. The flux J_{Fe_2B} and J_{Fe} are obtained from the Fick's First law as:

$$J_{Fe_2B}[x(t = t) = v, t = t] = -\left\{D_{Fe_2B}\partial C_{Fe_2B}[x(t = t) = v, t = t]/\partial x\right\}_{x = v}, \tag{5}$$

and

$$J_{Fe}[x(t = t) = v + dv,\ t = t] = -\left\{D_{Fe}\partial C_{Fe}[x(t = t) = v + dv,\ t = t]/\partial x\right\}_{x = v + dv}. \tag{6}$$

The term J_{Fe} is null since the boron solubility in the matrix is very low ($C_0 \approx 0$ mol m^{-3}) [25, 26]. Thus, Eq. (4) can be rewritten as follows:

$$\left(\frac{C_{up}^{Fe_2B} + C_{low}^{Fe_2B} - 2C_0}{2}\right)\left.\frac{dx(t)}{dt}\right|_{x(t) = v} = -D_{Fe_2B}\left.\frac{\partial C_{Fe_2B}[x(t = t), t = t]}{\partial x}\right|_{x(t) = v}. \tag{7}$$

If the boron concentration profile in Fe_2B is constant for the treatment time, the Fick's Second law is reduced to an ordinary second-order differential equation as follows:

$$\frac{\partial C_{Fe_2B}[x(t), t]}{\partial t} = D_{Fe_2B}\frac{\partial^2 C_{Fe_2B}[x(t), t]}{\partial x^2}. \tag{8}$$

By solving Eq. (8), and applying the boundary conditions proposed in Eqs. (2) and (3), the distribution of boron concentration through the Fe_2B layer is given by Eq. (9) if the boron diffusion coefficient in Fe_2B is constant for a particular temperature:

$$C_{Fe_2B}[x(t), t] = C_{up}^{Fe_2B} + \frac{C_{low}^{Fe_2B} - C_{up}^{Fe_2B}}{erf\left(\frac{v}{2\sqrt{D_{Fe_2B}t}}\right)} erf\left(\frac{x}{2\sqrt{D_{Fe_2B}t}}\right). \tag{9}$$

By substituting Eq. (9) into Eq. (7), Eq. (10) is obtained:

$$\left(\frac{C_{up}^{Fe_2B} + C_{low}^{Fe_2B} - 2C_0}{2}\right)\frac{dv}{dt} = \sqrt{\frac{D_{Fe_2B}}{\pi t}}\frac{C_{up}^{Fe_2B} - C_{low}^{Fe_2B}}{erf\left(\frac{v}{2\sqrt{D_{Fe_2B}t}}\right)}\exp\left(-\frac{v^2}{4D_{Fe_2B}t}\right), \tag{10}$$

for $0 \leq x \leq v$.

The Fe_2B layer thickness varies with the square root of time as follows:

$$v = 2\varepsilon D_{Fe_2B}^{1/2} t^{1/2}. \quad (11)$$

By substituting the derivative of Eq. (11) with respect to the time, Eq. (12) is obtained:

$$\left(\frac{C_{up}^{Fe_2B} + C_{low}^{Fe_2B} - 2C_0}{2}\right)\varepsilon = \sqrt{\frac{1}{\pi}}\frac{C_{up}^{Fe_2B} - C_{low}^{Fe_2B}}{erf(\varepsilon)}\exp(-\varepsilon^2). \quad (12)$$

The normalized growth parameter (ε) for the (Fe_2B/substrate) interface can be estimated numerically by the Newton–Raphson method [28]. It is assumed that the following boron concentrations: $C_{up}^{Fe_2B}$, $C_{low}^{Fe_2B}$, and C_0, do not depend significantly on temperature (in the considered temperature range) [19, 20, 22].

A schematic representation of the square of the Fe_2B layer thickness as a function of time ($v^2 = 4\varepsilon^2 D_{Fe_2B} t = 4\varepsilon^2 D_{Fe_2B}(t_v + t_0^{Fe_2B})$) is illustrated in Fig. 2 where $t_v(= t - t_0^{Fe_2B})$ is the effective growth time of the Fe_2B layer and t the treatment time.

3 Experimental Procedure

3.1 The Boriding Process

The AISI H13 steel was used as a substrate in the pack-boriding experiments. It has a nominal chemical composition of 0.32–0.45 % C, 0.80–1.20 % Si, 0.20–0.50 % Mn, 0.030 % P, 0.030 % S, 4.75–5.50 % Cr, 1.10–1.75 % Mo, 0.80–1.20 % V. The samples are cubic shaped of a nominal dimension of 10 mm × 10 mm × 10 mm. Before boriding, the samples were polished, ultrasonically cleaned in an alcohol solution and deionized water for 15 min at room temperature, and dried and stored under clean-room conditions. Then all samples to be borided were packed in a Durborid fresh powder mixture sealed in a stainless steel container (AISI 304. L). Boriding was performed in a conventional electrical resistance furnace under a pure argon atmosphere in the temperature range of 1,123–1,273 K. At the end of boriding process, the container was removed from the furnace and slowly cooled to room temperature.

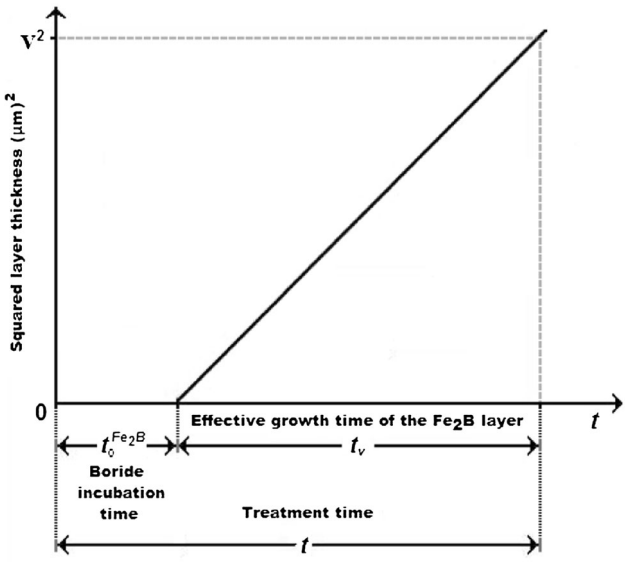

Fig. 2 Schematic representation of the square of the layer thickness against treatment time

3.2 Experimental Techniques

The microstructures of polished and etched cross-sections of the samples were observed by an Olympus GX51 optical microscope in a clear field and SEM (JEOL JSM 6300 LV). The boride layers thicknesses were automatically measured with the help of MSQ PLUS software. To ensure the reproducibility of the measured layers thicknesses, fifty measurements were collected in different sections of the borided samples to estimate the boride layer thickness; defined as an average value of the long boride needle [29–31]. Figure 3 schematically illustrates the practical procedure used to estimate the boride layers thicknesses.

The phases present in the boride layers were identified by an X-Ray Diffraction (XRD) equipment (Equinox 2000) using CoK_α radiation of 0.179 nm wavelength. The distribution of certain elements along a cross-section of the boride layer was determined by Electron Dispersive Spectroscopy (EDS) equipment (JEOL JSM 6300 LV) from the surface.

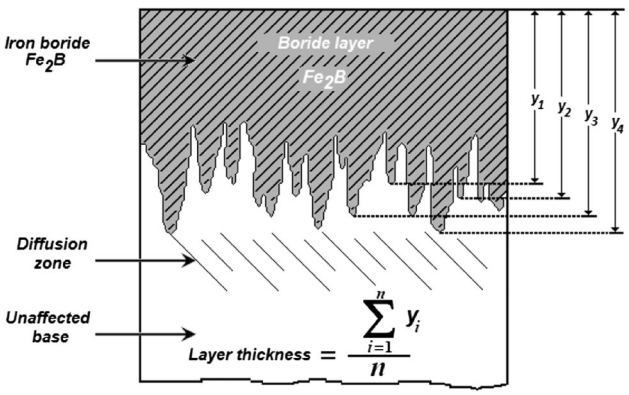

Fig. 3 Schematic diagram illustrating the procedure for estimation of boride layer thickness in AISI H13 steel

4 Results

4.1 OM Observations of the Boride Layers

Figure 4 shows the optical images of the cross-sections of borided layers at the surface of AISI H13 steel formed at 1,173 K for increasing treatment times. The obtained microstructure of boride layers are compact and continuous, having a flat interface.

4.2 SEM Observations and EDS Analysis

Figure 5a shows the SEM micrograph of the cross-section of boride layer formed at the surface of borided AISI H13 steel at 1,123 K for 4 h of treatment. The obtained boride layer exhibits a flat interface. The EDS analysis obtained by SEM is shown in Fig. 5b and c.

4.3 X-ray Diffraction Analysis

Figure 6 shows the XRD pattern recorded on the surface of borided AISI H13 steel at a temperature of 1,273 K for a treatment time of 8 h. The presence of Fe_2B was confirmed by XRD analysis where chromium borides such as CrB and Cr_2B were also detected.

4.4 Estimation of Boron Activation Energy

To determine the boron mobility in the Fe_2B layers, it is necessary to solve the mass balance equation at the (Fe_2B/substrate) interface (see Eq. (12)) using the Newton–Raphson numerical method [28]. The experimental results in terms of boride layers thicknesses are then needed to estimate the diffusion coefficients of boron in the Fe_2B layers by assuming the Arrhenius equation. Figure 7 shows the time dependence of the squared value of Fe_2B layer thickness for increasing temperatures. The values of growth constants $(=4\varepsilon^2 D_{Fe_2B})$ can be deduced from the slopes of the straight lines represented on Fig. 7.

Table 1 gathers the estimated value of boron diffusion coefficient in Fe_2B at each temperature along with the squared normalized value of ε parameter determined from Eq. (12).

The temperature dependence of boron diffusion coefficient in the Fe_2B layers is expressed by:

$$D_{Fe_2B} = D_0 \exp\left(\frac{-Q_{Fe_2B}}{RT}\right), \tag{13}$$

where D_0 is a pre-exponential constant, Q_{Fe_2B} the boron activation energy (J mol^{-1}), T the absolute temperature in Kelvin and $R = 8.314$ J mol^{-1} K^{-1} is the ideal gas constant. The activation energy for the boron diffusion in the boride layer was determined by the slopes obtained in the plot of ln D_{Fe_2B} versus $(1/T)$, using Eq. (14):

$$\ln D_{Fe_2B} = \ln D_0 - \frac{Q_{Fe_2B}}{RT}. \tag{14}$$

The temperature dependence of boron diffusion coefficient (in m^2 s^{-1}) though the Fe_2B layer was shown

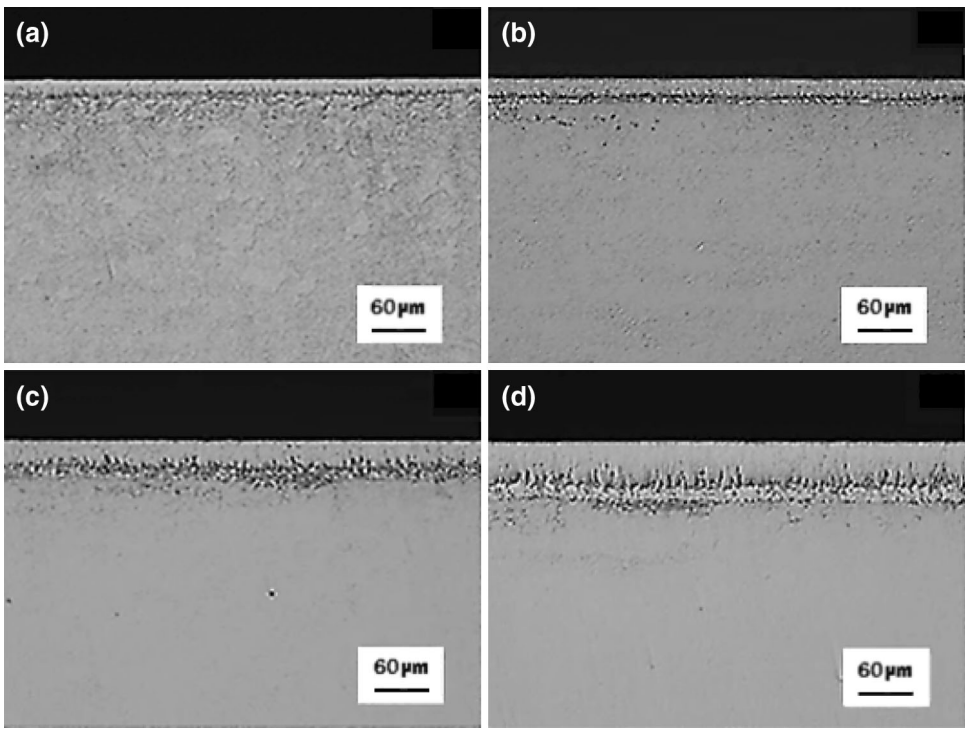

Fig. 4 Optical micrographs of the boride layers formed at the surface of AISI H13 steel treated at 1,173 K during a variable time: **a** 2 h, **b** 4 h, **c** 6 h and **d** 8 h

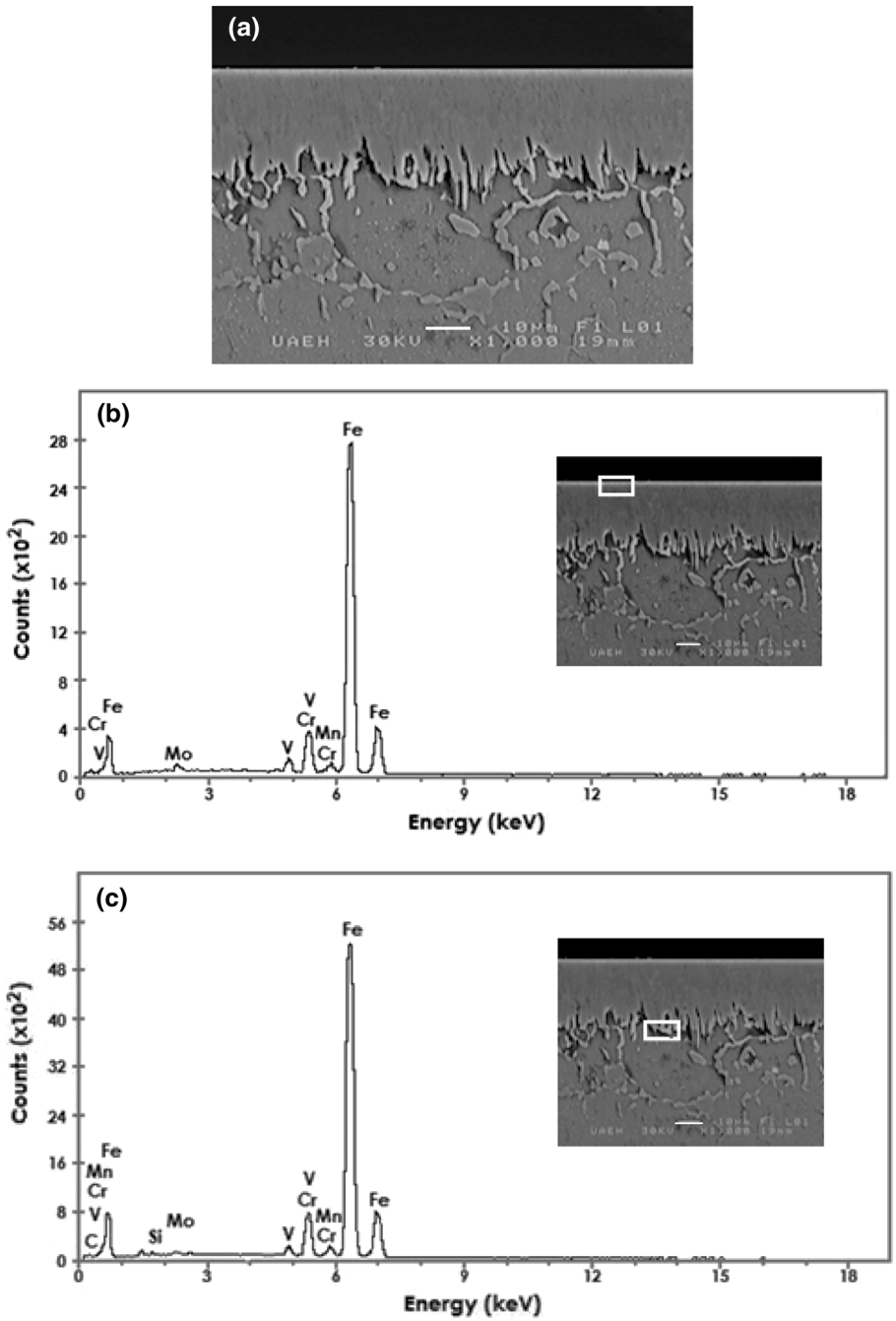

Fig. 5 **a** SEM micrographs of the cross-sections of the borided AISI H13 steel at 1,123 K for 4 h, **b** EDS spectrum of borided sample at surface and **c** EDS spectrum of borided sample at interface

in Fig. 8. A linear fitting was used to obtain Eq. (15) with a correlation factor of 0.9814.

$$D_{Fe_2B} = 3.0 \times 10^{-1} \exp\left(-\frac{233\,\text{kJ mol}^{-1}}{RT}\right). \quad (15)$$

This amount of energy is required to stimulate the boron diffusion along a [001] preferred direction due to the anisotropic nature of Fe_2B.

Table 2 compares the found boron activation energy for AISI H13 steel with other values for the borided AISI M2 and AISI H13 steels [32–36].

4.5 Validation of the Diffusion Model

The validation of the present model was achieved by comparing the experimental Fe_2B layer thickness with the

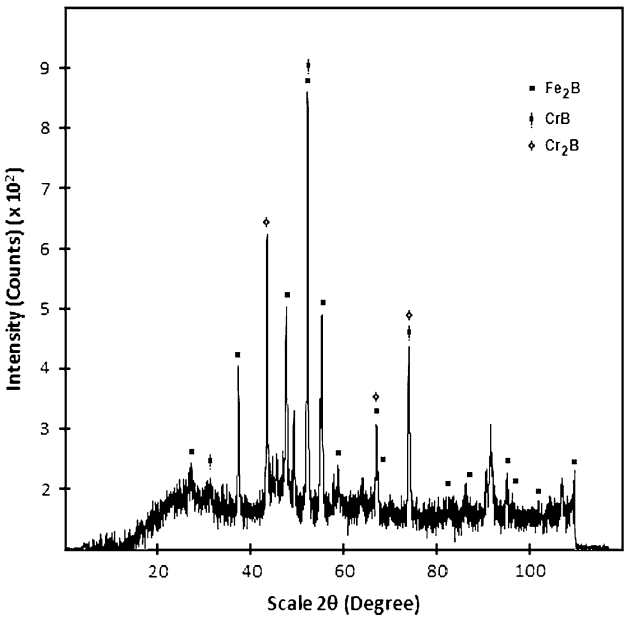

Fig. 6 XRD pattern obtained at the surface of the borided AISI H13 steel at 1,273 K for 8 h of treatment

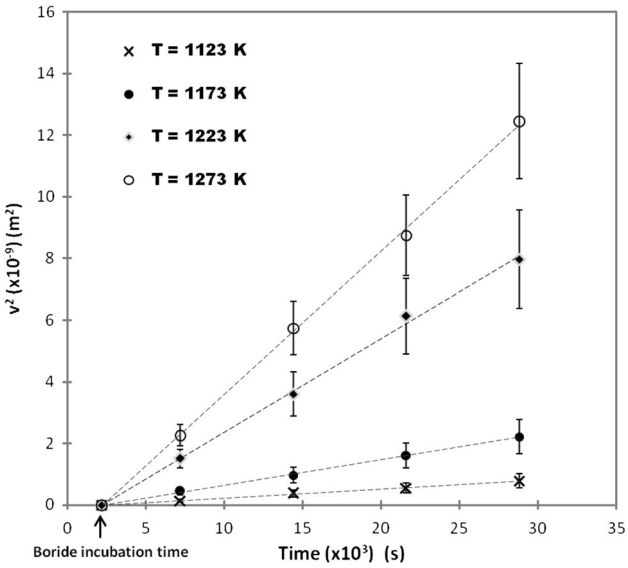

Fig. 7 The time dependence of the squared value of Fe_2B layer thickness at increasing temperatures

predicted value, obtained on the AISI H13 steel borided at 1,173 K during 7 h, 1,223 K during 5 h, 1,253 K during 2 h and 1,273 K for 3 h. Equation (16) predicts the experimental Fe_2B layer thickness for the given boriding conditions.

$$v = \sqrt{\frac{17 D_{Fe_2B} t}{2500}}. \quad (16)$$

Figure 9 shows the optical image of the Fe_2B layer formed at 1,173 K during 7 h, 1,223 K during 5 h, 1,253 K during 2 h and 1,273 K during 3 h of treatment.

Table 1 The squared value of normalized growth parameter and boron diffusion coefficients in Fe_2B as a function of boriding temperature

Temperature (K)	Type of layer	ε^2 (dimensionless)	$4\varepsilon^2 D_{Fe_2B}$ ($\mu m^2\ s^{-1}$)
1,123	Fe_2B	1.747141×10^{-3}	3.00×10^{-2}
1,173			8.00×10^{-2}
1,223			3.00×10^{-1}
1,273			5.00×10^{-1}

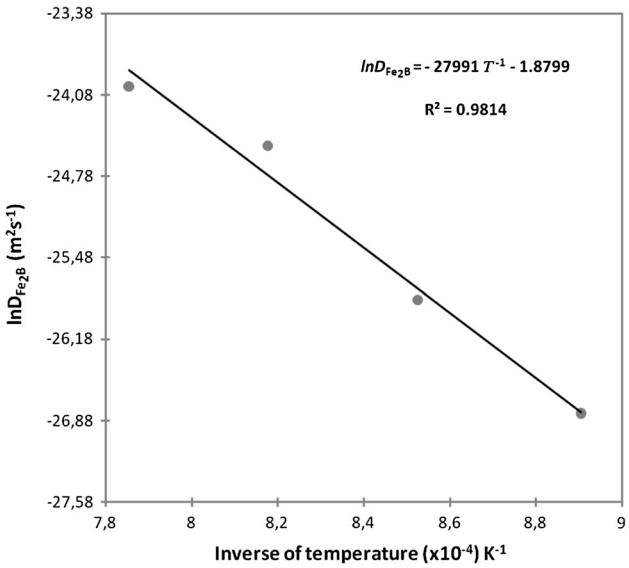

Fig. 8 The temperature dependence of boron diffusion coefficient in the Fe_2B layer

Table 3 compares between the experimental Fe_2B layers thicknesses and the predicted values using Eq. (16).

A good agreement was then obtained between the experimental values of Fe_2B layers thicknesses and the predicted results for the borided AISI H13 steel obtained at 1,173 K during 7 h, 1,223 K during 5 h, 1,253 K during 2 h and 1,273 K during 3 h of treatment. A contour diagram giving the evolution of Fe_2B layer thickness as a function of boriding parameters (time and temperature) is represented on Fig. 10.

5 Discussion

The H13 steel was pack-borided in the temperature range of 1,123–1,273 K for studying the kinetics of formation of Fe_2B layers. The XRD analysis confirmed the presence of Fe_2B phase besides the chromium borides such as CrB and Cr_2B. In this context, The XRD results reported by Genel [34] also indicated the existence of chromium borides (CrB

Table 2 A comparison of the boron activation energies for two borided steels

Material	Boriding method	Q_{Fe_2B} (kJ mol^{-1})	References
AISI H13	Salt-bath	244.37	[32]
AISI M2	Powder	207	[33]
AISI H13	Powder	186.2	[34]
AISI H13	Powder	213.92	[35]
AISI H13	Powder	189.6	[36]
AISI H13	Powder	233	Present study

Table 3 Predicted and estimated values of the Fe_2B layers thicknesses obtained at 1,173 K during 7 h, 1,223 K during 5 h, 1,253 K during 2 h and 1,273 K during 3 h of treatment

T(K)	Time (h)	Type of layer	Boride layer thickness (μm) estimated by Eq. (16)	Experimental boride layer thickness (μm)
1,173	7		46.50	41.54 ± 8.03
1,223	5	Fe_2B	64.05	61.11 ± 6.11
1,253	2		53.29	56.16 ± 9.36
1,273	3		77.81	74.08 ± 7.36

and Cr_2B) for the pack borided AISI H13 steel at 1,123 K for a treatment time of 1 h. The elements chromium and vanadium enter via a partial substitution into the lattice of the Fe_2B phase. In contrast, molybdenum has a much lower tendency to dissolve in the boride layer, tending to concentrate beneath the boride layer [37].

The microscopical examinations by OM and SEM revealed the formation of a single layer Fe_2B with a flat morphology. This particular morphology is attributed to the presence of the alloying elements in the substrate of AISI H13 steel and can be explained by the existence of activated diffusion pathways in the Fe_2B crystal lattice. It is known that the alloying elements modify the morphology of (boride layer/substrate) interface and tend to concentrate at the tips of the boride needles by generating a flat morphology. The concentration of the alloying elements also diminishes the active boron flux in this zone by reducing the boride layer thickness [38]. It is seen that the boride layer thickness varies with the treatment time. As a result, the boride layer thickness reached a value of 112.11 ± 19.2 μm for 8 h of treatment while its value was only 47.6 ± 17.7 μm for 2 h of treatment. The Fe_2B coating and its growth front are clearly distinguished from the steel matrix. A transition zone was also noticed beneath the boride layer in the optical micrographs of Fig. 4. The EDS analysis shows that chromium element dissolves in the Fe_2B phase, in fact, the atomic radius of Cr (=0.166 nm) is about the same and larger than that of Fe (=0.155 nm), and it can then be expected that Cr dissolved on the Fe sublattice of the borides. The concentration of manganese seems to be lower than that of iron in the boride layer due its lower solubility. The deficiency of Mn, Mo and V results in a negative effect on the boride layer in terms of both thickness and morphology. Figure 7c points out that carbon and silicon do not dissolve significantly over the Fe_2B phase and being displaced to the diffusion

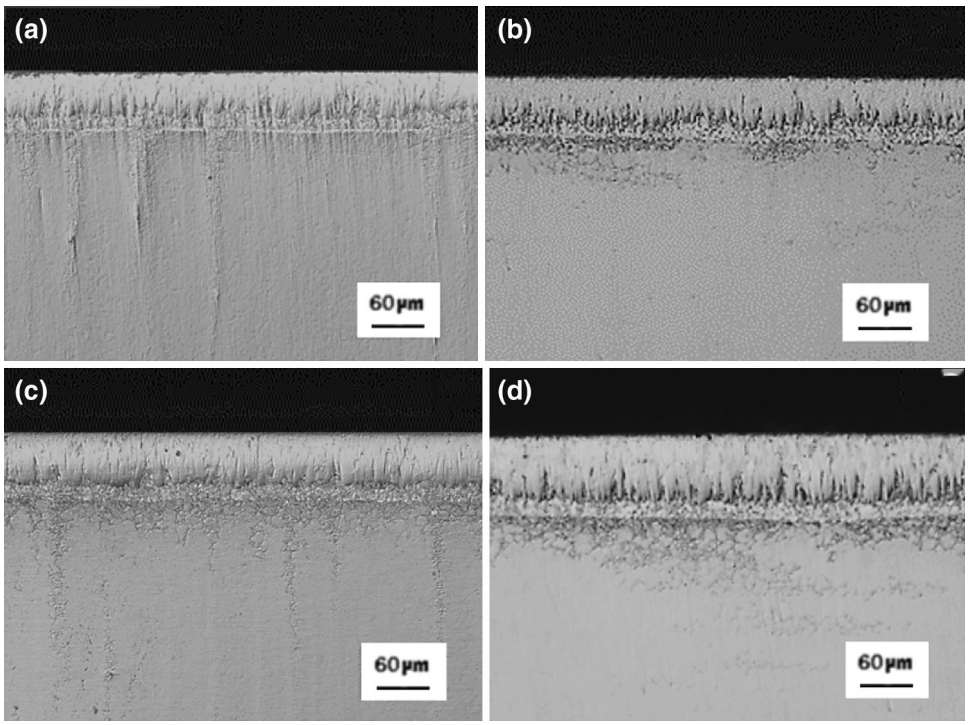

Fig. 9 Optical micrograph of the cross-section of the borided AISI H13 steel at: **a** 1,173 K for 7 h, **b** 1,253 K for 2 h and **c** 1,223 K for 3 h and **d** 1,273 K for 3 h of treatment

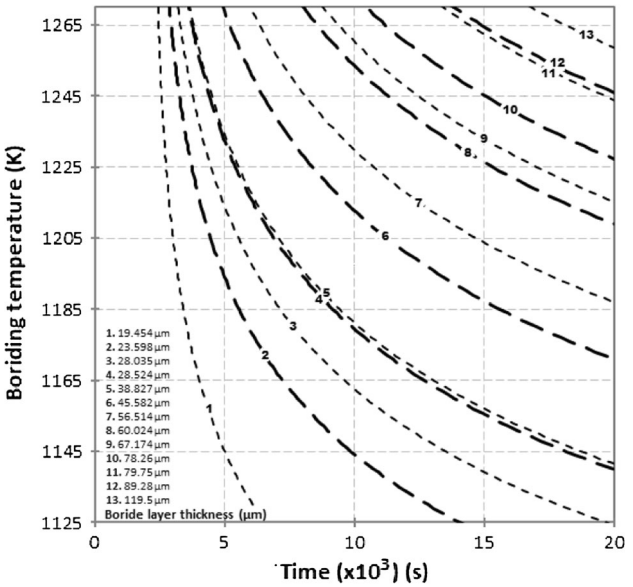

Fig. 10 Contour diagram describing the evolution of Fe_2B layer as a function of boriding parameters

zone, and forms together with boron, solid solutions like silicoborides ($FeSi_{0.4}B_{0.6}$ and Fe_5SiB_2) and boroncementite ($Fe_3Si_{0.67}B_{0.33}$) [39].

A diffusion model was suggested to estimate the boron diffusion coefficient in the Fe_2B phase according to the specified boriding conditions. The boron activation energy was deduced by adopting the Arrhenius relationship. The value of 233 kJ mol^{-1} was interpreted for the borided AISI H13 steel, as the amount of energy for the movement of boron atoms in the easiest path direction [001] along the boride layer that minimizes the growth stresses. This value of energy was then compared with the data available in the literature. So, the obtained value of boron activation energy (=233 kJ mol^{-1}) for AISI H13 steel was very comparable to that reported in the reference work [33] for the pack-boriding process. The estimated boron activation energies listed in Table 2 depended on the nature of boriding agent and the chemical composition of the substrate. In fact, the determination of the boron activation energy for the same borided steel depends on the method employed (either empirical approach or mathematical model). This value of energy can be interpreted as the required barrier to allow the boron diffusion inside the metal substrate. Thus the diffusion phenomenon of boron atoms can occur along the grains boundaries and also in volume to form the Fe_2B coating on the substrate. So the estimated value of boron activation energy for the AISI H13 steel is consistent with the data from the literature. The suggested diffusion model was validated by comparing the experimental Fe_2B layers thicknesses with the predicted values using Eq. (16) for the borided AISI H13 steel at 1,173 K during 7 h, 1,223 K during 5 h, 1,253 K during 2 h and 1,273 K for 3 h. A good concordance was observed between the experimental Fe_2B layer thickness and the predicted value by the model. The contour diagram presented on Fig. 10 can be used as a tool to select the optimum value of Fe_2B layer thickness in relation with the potential applications of the borided AISI H13 steel at industrial scale. As a rule, thin layers (e.g. 15–20 μm) are used to protect against adhesive wear (such as chipless shaping and metal stamping dies and tools), whereas thick layers are recommended to combat abrasive wear (extrusion tooling for plastics with abrasive fillers and pressing tools for the ceramic industry). In the case of low carbon steels and low alloy steels, the optimum boride layer thicknesses ranges from 50 to 250 μm, and for high-alloy steels, the optimum boride layer thicknesses ranges from 25 to 76 μm.

6 Conclusions

In this study, the boriding kinetics of Fe_2B layers on the AISI H13 steel was investigated in the temperature range of 1,123–1,273 K during a treatment time varying from 2 to 8 h. To determine the boron activation energy of AISI H13 steel, the mass balance equation was formulated under certain assumptions.

The estimated boron activation energy was found to be equal to 233 kJ mol^{-1}, and this result was compared with the literature data. The validity of the diffusion model was confirmed by comparing the experimental Fe_2B layers thicknesses obtained, at different temperatures and exposure times, with those predicted by the model. These predicted values were in good agreement with the experimental Fe_2B layers thicknesses.

In addition, a contour diagram was established to be used as a tool to select the optimum boride layer thickness according to the industrial utilization of this steel grade. As a further work, the present model can be extended for studying the growth kinetics of (FeB/Fe_2B) bilayer grown on any borided steel.

Acknowledgments The work described in this paper was supported by a grant of CONACyT and PROMEP México. Also, the authors want to thank Ing. Martín Ortiz Granillo, who is in charge as Director of the Escuela Superior de Ciudad Sahagún which belongs to the Universidad Autónoma del Estado de Hidalgo, México and Dr. Alejandro Domínguez, who is Coordinador del Programa para Apoyo a la Publicación de Investigaciones, Dirección de Desarrollo Curricular y Nuevos Productos and Vicerrectoría Académica UNITEC for all the facilities to accomplish this research work.

References

1. Sinha A K, *J Heat Treat* **4** (1991) 437.
2. Singhal S C, *Thin Solid Films* **45** (1977) 321.
3. Meric C, Sahin S, and Yilmaz S S, *Mater Res Bull* **35** (2000) 2165.

4. Pertek A, and Kulka M, *Appl Surf Sci* **202** (2002) 252.
5. Vipin J, and Sundararajan G, *Surf Coat Technol* **149** (2002) 21.
6. Keddam M, Kulka M, Makuch N, Pertek A, Małdziński L, *Appl Surf Sci* **298** (2014) 155.
7. Kukharev D S, Fizenko S P, and Shabunya S I, *J Eng Phys Thermophys* **69** (1996) 187.
8. Campos I, Oseguera J, Figueroa U, Garcia J A, Bautista O, and Keleminis G, *Mater Sci Eng A* **352** (2003) 261.
9. Keddam M, *Appl Surf Sci* **236** (2004) 451.
10. Campos-Silva I, Ortiz-Domínguez M, Villavelazquez C, Escobar R, and López N, *Defect Diffus Forum* **272** (2007) 79.
11. Campos-Silva I, López-Perrusquia N, Ortiz-Domínguez M, Figueroa-López U, Gómez-Vargas O A, Meneses-Amador A, and Rodríguez-Castro G, *Kovove Mater* **47** (2009)75.
12. Campos-Silva I, Ortiz-Domínguez M, Cimenoglu H, Escobar-Galindo R, Keddam M, Elías-Espinosa M, and López-Perrusquia N, *Surf Eng* **27** (2011) 189.
13. Ramdan R D, Takaki T, and Tomita Y, *Mater Trans* **49** (2008) 2625.
14. Keddam M, Ortiz-Domínguez M, Campos-Silva I, and Martinez-Trinídad J, *Appl Surf Sci* **256** (2010) 3128.
15. Ortiz-Domínguez M, Hernandez-Sanchez E, Martinez-Trinídad J, Keddam M, and Campos-Silva I, *Kovove Mater* **48** (2010) 1.
16. Keddam M, and Chegroune R, *Appl Surf Sci* **256** (2010) 5025.
17. Nait Abdellah Z, Keddam M, Chegroune R, Bouarour B, Haddour L, and Elias A, *Matér Tech* **100** (2012) 581.
18. Nait Abdellah Z, Keddam M, and Elias A, *Int J Mater Res* **104** (2013) 260.
19. Ortiz-Domínguez M, Keddam M, Elias-Espinosa M, Damián-Mejía O, Flores-Rentería M A, Arenas-Flores A, and Hernández-Ávila J, *Surf Eng* **30** (2014) 490.
20. Elias-Espinosa M, Ortiz-Domínguez M, Keddam M, Flores-Rentería M A, Damián-Mejía O, Zuno-Silva J, Hernández-Ávila J, Cardoso-Legorreta E, and Arenas-Flores A, *J Mater Eng Perform* **23** (2014) 2943.
21. Kulka M, Makuch N, Pertek A, and Maldzinski L, *J. Solid State Chem* **199** (2013) 196.
22. Brakman C M, Gommers A W J, and Mittemeijer E J, *J Mater Res* **4** (1989) 1354.
23. Massalski T B, *Binary Alloys Phase Diagrams*, 2nd Edn., ASM International, Materials Park, OH (1990).
24. Yu L G, Chen X J, Khor K A, and Sundararajan G, *Acta Mater* **53** (2005) 2361.
25. Okamoto H, *J Phase Equilib Differ* **25** (2004) 297.
26. Nait Abdellah Z, Chegroune R, Keddam M, Bouarour B, Haddour L, and Elias A, *Defect Diffus Forum* **322** (2012) 1.
27. Dybkov V I, *Reaction Diffusion and Solid State Chemical Kinetics*, Trans Tech Publications, Dürnten (2010) p 7.
28. Press W H, Flanery B P, and Teukolsky S A, *Numerical Recipes in Pascal: The Art of Scientific Computing*, Cambridge University, Cambridge (1989).
29. Campos-Silva I, Bravo-Bárcenas D, Meneses-Amador A, Ortiz-Dominguez M, Cimenoglu H, Figueroa-López U, and Andraca-Adame J, *Surf Coat Technol* **237** (2013) 402.
30. H. Kunst, O. Schaaber, *Härterei-Tech Mitt* **22** (1967) 275.
31. Campos-Silva I, Ortiz-Domínguez M, Bravo-Bárcenas O, Doñu-Ruiz M A, Bravo-Bárcenas D, Tapia-Quintero C, and Jiménez-Reyes M Y, *Surf Coat Technol* **205** (2010) 403.
32. Taktak S, *J Mater Sci* **41** (2006) 7590.
33. Campos-Silva I, Ortiz-Domínguez M, Tapia-Quintero C, Rodríguez-Castro G, Jiménez-Reyes M Y, and Chávez-Gutiérrez E, *J Mater Eng Perform* **21** (2012) 1714.
34. Genel K, *Vacuum* **80** (2006) 451.
35. Xu L, Wu X, and Wang H, *J Mater Sci Technol* **23** (2007) 525.
36. Campos-Silva I, Ortiz-Domínguez M, López-Perrusquia N, Bermúdez-Rodríguez G, and Gómez-Vargas O A, *Defect Diffus Forum* **283–286** (2009) 681.
37. Badini C, Gianoglio G, and Pradelli G, *Surf Coat Technol* **30** (1987), 157.
38. Nait Abdellah Z, Keddam M, and Elias A, *Acta Phys Pol A* **122** (2012) 588.
39. Dukarevich I S, Mozharov M V, and Shigarev A S, *Metallovedenie Termicheskaya I Obrabotka Metallov* **2** (1973) 64.